HHS Public Access

Author manuscript

J Am Chem Soc. Author manuscript; available in PMC 2023 August 16.

Published in final edited form as:

J Am Chem Soc. 2022 March 09; 144(9): 4196–4205. doi:10.1021/jacs.2c00007.

Insights into the Cross Talk between Effector and Allosteric Lobes of KRAS from Methyl Conformational Dynamics

Fa-An Chao,
NCI RAS Initiative, Cancer Research Technology Program, Frederick National Laboratory for Cancer Research, Leidos Biomedical Research, Frederick, Maryland 21701, United States

Srisathiyanarayanan Dharmaiah,
NCI RAS Initiative, Cancer Research Technology Program, Frederick National Laboratory for Cancer Research, Leidos Biomedical Research, Frederick, Maryland 21701, United States

Troy Taylor,
NCI RAS Initiative, Cancer Research Technology Program, Frederick National Laboratory for Cancer Research, Leidos Biomedical Research, Frederick, Maryland 21701, United States

Simon Messing,
NCI RAS Initiative, Cancer Research Technology Program, Frederick National Laboratory for Cancer Research, Leidos Biomedical Research, Frederick, Maryland 21701, United States

William Gillette,
NCI RAS Initiative, Cancer Research Technology Program, Frederick National Laboratory for Cancer Research, Leidos Biomedical Research, Frederick, Maryland 21701, United States

Dominic Esposito,
NCI RAS Initiative, Cancer Research Technology Program, Frederick National Laboratory for Cancer Research, Leidos Biomedical Research, Frederick, Maryland 21701, United States

Dwight V. Nissley,
NCI RAS Initiative, Cancer Research Technology Program, Frederick National Laboratory for Cancer Research, Leidos Biomedical Research, Frederick, Maryland 21701, United States

Frank McCormick,
Helen Diller Family Comprehensive Cancer Center, University of California San Francisco, San Francisco, California 94158, United States

R. Andrew Byrd,
Center for Structural Biology, Center for Cancer Research, National Cancer Institute, Frederick, Maryland 21702, United States

Corresponding Authors Fa-An Chao – NCI RAS Initiative, Cancer Research Technology Program, Frederick National Laboratory for Cancer Research, Leidos Biomedical Research, Frederick, Maryland 21701, United States; fa-an.chao@nih.gov; Gabriel Cornilescu – NCI RAS Initiative, Cancer Research Technology Program, Frederick National Laboratory for Cancer Research, Leidos Biomedical Research, Frederick, Maryland 21701, United States; gabriel.cornilescu@nih.gov.

Supporting Information

The Supporting Information is available free of charge at https://pubs.acs.org/doi/10.1021/jacs.2c00007.
Additional figures and primary experimental data (PDF)

The authors declare no competing financial interest.

Dhirendra K. Simanshu,
NCI RAS Initiative, Cancer Research Technology Program, Frederick National Laboratory for Cancer Research, Leidos Biomedical Research, Frederick, Maryland 21701, United States

Gabriel Cornilescu
NCI RAS Initiative, Cancer Research Technology Program, Frederick National Laboratory for Cancer Research, Leidos Biomedical Research, Frederick, Maryland 21701, United States

Abstract

KRAS is the most frequently mutated RAS protein in cancer patients, and it is estimated that about 20% of the cancer patients in the United States carried mutant RAS proteins. To accelerate therapeutic development, structures and dynamics of RAS proteins had been extensively studied by various biophysical techniques for decades. Although ^{31}P NMR studies revealed population equilibrium of the two major states in the active GMPPNP-bound form, more complex conformational dynamics in RAS proteins and oncogenic mutants subtly modulate the interactions with their downstream effectors. We established a set of customized NMR relaxation dispersion techniques to efficiently and systematically examine the ms-μs conformational dynamics of RAS proteins. This method allowed us to observe varying synchronized motions that connect the effector and allosteric lobes in KRAS. We demonstrated the role of conformational dynamics of KRAS in controlling its interaction with the Ras-binding domain of the downstream effector RAF1, the first kinase in the MAPK pathway. This allows one to explain, as well as to predict, the altered binding affinities of various KRAS mutants, which was neither previously reported nor apparent from the structural perspective.

Graphical Abstract

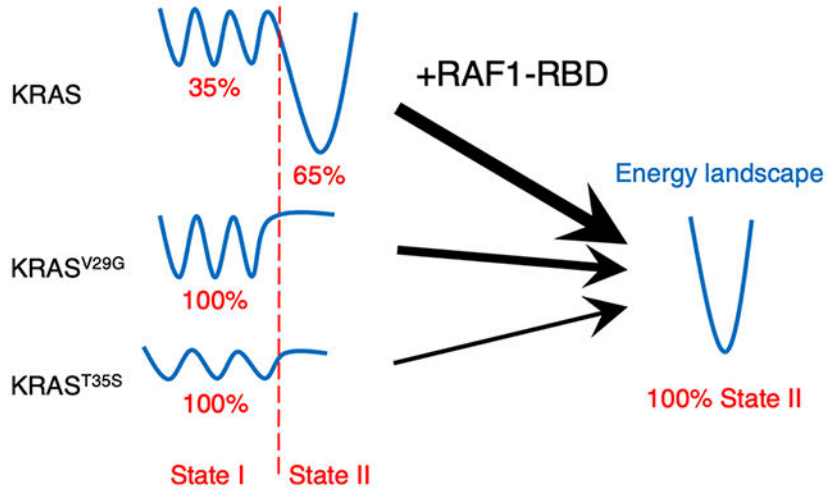

INTRODUCTION

The RAS protein family is a class of a membrane-associated GTPase protein that cycles between a GDP-bound (inactive) form and a GTP-bound (active) form during signal transduction.[1] It was estimated that ~20% of the cancer patients in the United States carried

mutant RAS proteins with ~3.4 million new cases per year.[2] Among the RAS proteins—HRAS, NRAS, and KRAS—oncogenic mutations are predominantly detected at amino acid positions G12, G13, and Q61.[3] KRAS is expressed as alternatively spliced major KRAS4b and minor KRAS4a isoforms and is responsible for 86% of RAS-driven cancers, including pancreatic, colorectal, and lung cancers.[3] Although the RAS protein was initially thought to be undruggable, new therapeutic developments allow targeting of the KRAS oncogenic mutation G12C.[4,5]

RAS proteins contain a highly conserved GTPase domain (G-domain; a.a. 1–166) and a hypervariable region (HVR; a.a. 167–188/189).[1] The HVR undergoes post-translational modification, which anchors RAS to the plasma membrane. The G-domain (1–166) is composed of two lobes—effector and allosteric.[6] The effector lobe is formed by residues 1–86 and is fully conserved across all RAS isoforms. The allosteric lobe comprises residues 87–166 and has 90% sequence identity among the RAS isoforms. Extensive structural studies[6,7] have demonstrated that the G-domains of all RAS proteins share the same fold, and the systematic structural analysis[1] of GDP-bound and GTP-bound forms shows structural changes mainly in the two regions referred to as switch I (residues 30–38) and switch II (residues 60–76). Based on crystal structures[8,9] and ^{31}P solution-state nuclear magnetic resonance spectroscopy (NMR) studies of RAS bound to the non-hydrolyzable GTP analog, GMPPNP,[9,10] two dominant conformational states were identified in the switch I. These are defined as state I (open state) and state II (closed state). ^{31}P NMR studies[10] have shown that wild-type RAS proteins are in equilibrium between states I and II, with state II being the major conformer. Many mutations on the switch I region[11] alter the population distribution toward the state I conformation with clear effects on the binding affinities to the effector proteins. Residues in the switch I region of RAS interact with the Ras-association or Ras-binding domain (RBD) of effector proteins,[12] and the formation of a RAS–effector complex locks the switch I region in the state II conformation in wild-type as well as in oncogenic mutants of RAS.[10,11] Stabilizing the state I conformation of the switch I region of RAS has been proposed as a potential therapeutic approach for preventing RAS–effector interactions.[13,14]

Multiple studies[10,15-17] have shown that solution-state NMR is an effective tool to investigate the conformational exchange between the two conformational states, state I and state II, in HRAS. A recent NMR study[18] on a RAS-related protein Rac1 also demonstrated the strong correlation between the populations of these conformational states and the oncogenic activity of Rac1 mutant proteins. Systematic studies of other RAS proteins and their mutants are still lacking despite noticeable biochemical differences among the different RAS isoforms.[19] Previous studies[9,11] have shown that mutations of residues present in the switch I region (T35A, T35S, and V29G) shift the HRAS protein toward the state I conformation, which can significantly affect the binding affinity for the RBD of various RAS effectors. Residue T35 coordinates with the Mg^{2+} ion via its side-chain hydroxyl and interacts with the γ-phosphate via its main-chain amide nitrogen in the state II conformation.[8] The population distribution between states I and II is affected by the change in interactions of T35 with Mg^{2+} and the γ-phosphate, and T35 mutants, such as T35S and T35A, are predominantly in the state I conformation.[9] On the other hand, residue V29, located at the beginning of the flexible switch I region, may act as a hinge. Consequently, the

V29G mutation favors the state I conformation[11] likely by increasing the switch I region's flexibility. Although ^{31}P NMR studies [10,11] on RAS proteins provide valuable information regarding the population equilibrium of the two major states in the active GMPPNP-bound form, new approaches need to be explored to quantitatively reveal the potentially complex functional effects elicited by conformational dynamics in RAS proteins, as suggested by high-pressure NMR studies[20,21] and enhanced molecular dynamic (MD) simulations.[6,7,22]

Here, we utilize selectively isotope-labeled methyl groups in a highly deuterated background to quantitatively study the dynamic exchange among multiple conformational states of the G-domain of KRAS4b (referred from hereon as KRAS) in solution. First, combining different methyl relaxation dispersion techniques,[23-25] we demonstrate that selected methyl groups in KRAS allow the simultaneous probing of conformational exchange of the switch I region in both GDP-bound and GMPPNP-bound forms. Using this approach, we observe a strong coupling of conformational dynamics between the effector and allosteric lobes in wild-type KRAS proteins in the GMPPNP-bound form. The sensitivity-enhanced methyl NMR experiments allow the screening of conformational dynamics of different RAS mutants using shorter NMR acquisition time and/or less isotope-labeled protein. To further dissect complex ms-μ conformational dynamics, we investigated these mutants stabilizing the state I conformation (T35A, T35S, and V29G) in the GMPPNP-bound form. We observed a reduced degree of coupled conformational dynamics between the effector and allosteric lobes in KRAS^{V29G}, compared to wild type, while no coupling is observed in KRAS^{T35S}. Furthermore, the exchange rates between different conformational states and the energy barriers among populated conformational states are strongly correlated with the binding affinity of KRAS to RAF1-RBD. Finally, in addition to ^{31}P NMR data, we present a set of customized experiments to provide a more complete picture of conformational dynamics in KRAS proteins, with a potential value for future therapeutic developments since KRAS–effector interactions are clearly modulated by its dynamic behavior.

MATERIALS AND METHODS

Sample Preparation.

All isotopic precursors were from Cambridge Isotopic Laboratories, Inc. (Tewksbury, MA, USA). Alpha-ketobutyric acid,[26] sodium salt (methyl-^{13}C, 99%; 3,3-D2, 98%, CDLM-7318), D-glucose (1,2,3,4,5,6,6-D7 97–98%, DLM-2062), and ammonium chloride (^{15}N, 99%, NLM-467) were used. DNA constructs for the expression of Gly-Hs.KRAS4b (1–169) (Addgene #159539) and Hs.RAF1(52–131) were previously described.[27] Mutant forms of KRAS were synthesized using clones from the KRAS Mutant Entry clone library (Addgene) as templates. All expression constructs were in the form containing an N-terminal His6 and maltose-binding protein (MBP) tag (Addgene #11517). RAF1- RBD (52–131) was expressed using the auto-induction media protocol,[28] and KRAS proteins were expressed using the previously published protocol.[28] Highly deuterated and ^{13}C-methyl-labeled KRAS proteins were expressed using the following protocol. Specifically, a BL21 STAR (*rne*131) *Escherichia coli* strain containing the DE3 lysogen and rare tRNAs (pRare plasmid Cm^{R}) was transformed with an expression plasmid (Amp^{R}). An isolated and purified transformant was used to create a glycerol stock. An *E. coli* seed culture was

inoculated from a glycerol stock and grown in 50 mL of MDAG medium[28] in a 250 mL baffled shake flask for 16 h at 37 °C until mid-log phase growth. Thirty milliliters of the mid-log phase culture was used to inoculate 300 mL of LB Miller medium with antibiotics in a 2 L baffled shake flask and grown at 37 °C at 250 RPM. After 1 h of growth, 300 mL of 100% D_2O ModM9 (33.5 mM Na_2HPO_4, 44.1 mM KH_2PO_4, 17.1 mM NaCl, 11.1 mM glucose, 18.7 mM NH_4Cl, 2 mM $MgSO_4$, 100 μM $CaCl_2$, 4 μM $ZnSO_4$, 1 μM MnSO4, 4.7 μM H3BO_3, and 0.7 μM $CuSO_4$) with antibiotics was added and growth was continued for an additional 1 h. Six hundred milliliters of 100% D_2O ModM9 with antibiotics was then added, and the 1200 mL total volume was poured into a 4 L baffled shake flask and grown for an additional 2 h. The culture was centrifuged at 4000g for 15 min at 25 °C. Cell pellets were resuspended with 6 L of 90:10 D_2O:H_2O ModM9 with antibiotics and modifications (11.1 mM deuterated glucose, 18.7 mM ^{15}NH4Cl, and 393 μM alpha-ketobutyric acid (methyl ^{13}C)) and grown to an OD_{600} of 0.5. Protein expression was induced with 0.5 mM IPTG, and grown for an additional 17 h at 16 °C or for 3 h at 37 °C. Cells were collected by centrifugation at 5000g for 20 min at 4 °C and stored at −80 °C. Similarly, deuterated Hs.RAF1(52–131) was expressed as outlined above with overnight induction at 16 °C but without the addition of other isotopes to the final 6 L of 90:10 D_2O:H_2O ModM9 cell resuspension. All proteins were purified as described previously[29] for constructs of the format His6-MBP-tev-protein of interest (POI). Purified GDP-bound wild-type and mutants of KRAS were exchanged to GMPPNP-bound forms using the procedure reported earlier.[27]

NMR Data Collection.

All methyl relaxation dispersion experiments were performed using U-[^{15}N, ^{2}H], $^{13}CH_3$-δ_1Ile-labeled wild-type, and mutant KRAS4b samples (1–169) with a concentration of about 250 μM in a 20 mM HEPES (pH 7.4), 150 mM NaCl, 5 mM $MgCl_2$, and 2 mM TCEP buffer. All relaxation dispersion experiments were carried out using Bruker Avance III spectrometers equipped with a helium-cooled TCI cryoprobe at 800 MHz (18.8 T) or at 850 MHz (20 T) or using a Bruker Avance NEO spectrometer equipped with a helium-cooled TCI cryoprobe at 700 MHz (16.4 T). All experimental temperatures were calibrated using a standard sample, Methanol-d_4. The sensitivity-enhanced carbon single-quantum CPMG experiments[23] were carried out with a 20 ms constant time, 2 s recycle delay, 48 scans, 50 complex points in the ^{13}C dimension (8 ppm), and 2048 complex points in the ^{1}H dimension (14 ppm). A γB_1 frequency of ~ 15 kHz was used for the ^{13}C π pulse in the constant-time spinecho period, with ν_{CPMG} values of 100, 200, 400, 500, 800, and 1000 Hz, with repetition of the 100, 400, and 1000 Hz data points. The offresonance effects of the π pulses in CPMG experiments in this case can be largely ignored due to the small ^{13}C spectral window (±700 Hz at 700 MHz), and all CPMG experiments were acquired at 700 MHz, unless stated otherwise. A complete CPMG data set required an acquisition time of about 14 h for each temperature, and data were processed with linear prediction of an additional 50 complex points in the ^{13}C dimension using NMRPipe[30] and subsequently analyzed by Sparky.[31] Similarly, the adiabatic relaxation dispersion experiments[24] were carried out with a 2 s recycle delay, 8–16 scans, 50 complex points in the ^{13}C dimension (8 ppm), and 2048 complex points in the ^{1}H dimension (14 ppm). All experimental parameters in the spin-lock period with adiabatic hyperbolic secant shape pulses[24] (HS) and composite pulse proton decoupling[25] were set as previously published (available in the Bruker user library), and

all the adiabatic experiments were carried out at high magnetic fields (800 or 850 MHz) to further expand the detectable range of conformational exchange regimes. Total relaxation delays (N = 0, 2, 4, and 6) were 0, 32, 64, and 96 ms for the adiabatic $R_{1\rho}$ experiments and 0, 16, 48, and 80 ms (N = 0, 1, 3, and 5) for the adiabatic $R_{2\rho}$ experiments. The relaxation delays for the R_1 experiments were 0.0, 0.05, 0.1, 0.15, and 0.2 s, repeating the 0.0, 0.1, and 0.2 s delays. The relaxation delays for the R_2 experiments were 0, 20, 40, 60, and 80 ms, repeating 0, 40, and 80 ms delays. Data were processed similarly to the CPMG experiments. A complete set of adiabatic relaxation dispersion data consisted of R_1, R_2, adiabatic $R_{1\rho}$, and adiabatic $R_{2\rho}$ experiments, requiring approximately 12–24 h of total acquisition time for each temperature. All the above relaxation dispersion experiments were performed at a single magnetic field strength at three different temperatures and were run interleaved to minimize systematic experimental errors due to eventual protein sample instability. All the previously published pulse sequences were modified with 3919 WATERGATE and/or CW presaturation to suppress the solvent signal at various temperatures.

The products of S^2 and τ_c of labeled methyl groups were measured via analyzing the buildup of ^1H triple-quantum magnetization with respect to single-quantum relaxation,[32] using 5, 10, 15, 20, 25, 30, 35, 40, and 45 ms delays, repeating the 5, 20, and 45 ms delays. The global rotation correlation times τ_c of different KRAS protein samples were determined using TRACT experiments.[33]

Data Analysis of Relaxation Dispersion Experiments.

As described in the main text, all relaxation dispersion data were analyzed in a site-specific manner, using a simple 2-site exchange model. On our instruments, for the given experimental settings (with well-calibrated π pulses), we estimated the experimental errors of effective R_2 rates to be $\pm 1\ s^{-1}$ and we set $3\ s^{-1}$ as the detection limit of the CPMG experiments. Amplitude of the relaxation dispersion profile smaller than $3\ s^{-1}$ will not be included in the following data analysis. In the case of SQ-CPMG data, an in-house python script was built using the exact analytic solution[34] and a search algorithm similar to the one used by the NESSY[35] software, which starts with an extensive grid search and ends with an accelerated gradient descent. While searching for the minimal deviation of theoretical values from the experimental data at different temperatures, the Arrhenius equation and a fixed $\Delta\omega$ value were imposed as additional restraints. Here, the Arrhenius equation simply restrains the linearity of the inverse temperature dependence of the logarithm of the reaction rates (k_1 and k_{-1}). The best 10 results from 100 independent fits were used to provide average values of the dynamic parameters and their standard deviations. To analyze the adiabatic relaxation dispersion data, we followed the previously published method that uses numerically simulated solution libraries[24] (available in NMRbox[36]). Moreover, the previously published algorithm was modified to incorporate the assumptions of the Arrhenius equation and a fixed $\Delta\omega$ value at different temperatures during data fitting, as well as to output a χ^2 surface for an array of input dynamic parameters. Since it is difficult to estimate the experimental errors for this type of experiment, we first confirmed detected conformational exchanges by monitoring the variations of χ^2 surfaces at different temperatures. Lower χ^2 values result in a better fit of the experimental data. Thus, we analyzed and reported exchange rates (k_{ex}) only when a trend was observed that k_{ex} rates with the lowest χ^2 values decrease

as the temperature decreases for a given methyl group. As suggested previously,[24] the 40 results with the best scores from 100 independent fits were used to provide average values of the dynamic parameters and their standard deviations. The confident exchange rates (k_{ex}) were reported when their standard deviations from the 40 outputs are less than 0.3 in the logarithm scale. Finally, in the analysis of relaxation dispersion data, all intrinsic relaxation rates at different temperatures were treated as independent variables.

ITC Measurements.

A MicroCal PEAQ-ITC calorimeter (Malvern) was used to perform ITC binding studies. GMPPMP-bound KRAS4b or its mutants and the RAF1-RBD domain were extensively dialyzed in the same buffer containing 20 mM HEPES (pH 7.3), 150 mM NaCl, 5 mM $MgCl_2$, and 1 mM TCEP. This dialysis buffer was also used for any protein dilutions for the following ITC runs. The concentrations of the proteins were measured using absorbance at 280 nm in a NanoDrop 2000c spectrophotometer (Thermo Fisher Scientific). Before each ITC run, protein samples were centrifuged at 14,000g for 5 min at 4 °C to remove any debris and air bubbles. For ITC titrations, the concentrations of RAF1-RBD and KRAS4b were 650 and 60 μM, respectively. ITC titrations were performed by an initial injection of 0.4 μL followed by 18 injections of 2.2 μL of RAF1-RBD proteins at 150 s intervals into a cell containing KRAS4b proteins. Data obtained from the calorimeter are imported into MicroCal PEAQ-ITC analysis software and subsequently analyzed to obtain thermodynamic parameters (ΔG, ΔH, and $-T\Delta S$), curve fitting, equilibrium dissociation constant, and molar ratio calculations.

RESULTS

Effects of γ-Phosphate on ms-μ Dynamics of Wild-Type KRAS.

Methyl groups have been shown to be powerful probes[37,38] to investigate conformational dynamics in large protein complexes using solution-state NMR spectroscopy. Previous studies[39,40] showed that the ^{13}C isotope-labeled δ_1 methyl group of isoleucine residues in KRAS provide highly sensitive and well-dispersed NMR spectra in both GDP-bound and GMPPNP-bound forms (Figure S1), while the amide signals of the switch I region in the GMPPNP-bound form are not detectable due to conformational exchange broadening. Using the δ_1 methyl group of isoleucine residues as probes of conformational dynamics, we first examined wild-type KRAS using ^{13}C single-quantum Carr-Purcell-Meiboom-Gill (SQCPMG) experiments.[23] Classic CPMG experiments allow the detection of conformational exchange phenomena on the ms-μs timescale by observing changes in relaxation rates when varying the frequency of a series of π pulses (ν_{CPMG}). The confidence in the extracted dynamic parameters is proportional to the magnitude of the change in relaxation rates (or amplitude of the relaxation dispersion profile). Large amplitudes of relaxation dispersion profiles of many labeled methyl groups (7 out of 11) could be easily detected in GMPPNP-bound KRAS at 25 °C (Figure 1A and Figure S2). In contrast, we detected little or no dispersion profiles ($<3\ s^{-1}$) in GDP-bound KRAS, even when using sensitive multiple-quantum (MQ) CPMG experiments[41] due to methyl-TROSY effects (Figure S2A). To observe exchange events outside of the detectable window of standard

CPMG techniques, we employed sophisticated methyl adiabatic relaxation dispersion experiments[24,25] to detect cases of conformational exchange in the GDP-bound form.

In the switch I region, under the assumption of a two-site exchange between state I and state II, we found that the presence of conformational exchanges in both the GMPPNP-bound form (detected by methyl ^{13}C SQ-CPMG) and GDP-bound form (detected by methyl ^{13}C adiabatic relaxation dispersion) can be observed using a single methyl group of residue I-36 (Figure 1B). Although the detected exchange rates of I-36 in the GMPPNP-bound form at different temperatures are slower than those previously reported in HRAS, the temperature-dependent variation of the exchange rates (or the slope of this linear dependence) is almost identical to the one extracted previously by line shape analysis in the ^{31}P NMR spectra of HRAS[10] (Figure 1B), which suggests that both experiments detected the same conformational exchange in the switch I region. We also found that the reported minor population (~5% in the state I) at I-36 in the GMPPNP-bound form using SQ-CPMG experiments (Figure S3) is much lower than the one (~35%) reported by ^{31}P NMR studies.[10,40] Based on a previous study,[42] the underestimation of the minor population can result from the analysis of relaxation dispersion experiments in complex exchange phenomena with too simplistic exchange models. Thus, the inconsistency between our reported minor population and the previously reported one suggests the presence of more complex conformational exchange phenomena. On the other hand, we found that the exchange rates of the same methyl group of I-36 in the GDP-bound form at different temperatures are an order of magnitude faster than the one reported in HRAS using amide ^{1}H CPMG experiments[17] (Figure 1B). Thus, the above results demonstrated that the combined methyl SQ-CPMG and adiabatic relaxation dispersion techniques allow observation of an ultra-broad range of conformational exchange rates and their temperature-dependent variations in KRAS proteins.

Next, we explored the conformational dynamics of other ^{13}C-labeled methyl groups in wild-type KRAS. As indicated by previous high-pressure NMR studies[20,21] and by our CPMG data analysis for I-36, we expected complex conformational exchanges in KRAS, with different methyl groups experiencing different types of motions. To simplify the data analysis of these complex conformational exchanges, we applied the following strategy in analyzing the relaxation dispersion results: each methyl group data set is fitted separately, assuming a simple two-site exchange model with reaction rates (k_1 and k_{-1}) following the Arrhenius equation, as well as a fixed chemical shift difference ($\Delta\omega$) at different temperatures. The calculated exchange rates ($k_{ex} = k_1 + k_{-1}$) and their temperature-dependent variations are monitored when the system is perturbed. This strategy not only allows the identification of synchronized and collective motions dominant in the relaxation dispersion profiles but also enables detection of changes in a protein experiencing complex conformational dynamics.

The methyl groups of residues I-21, I-24, I-36, and I-55 in the effector lobe of KRAS, which show large relaxation dispersion profiles in the GMPPNP-bound form, were first selected for further analysis (Figure 1A). In the GDP-bound form, although only two methyl groups (I-36 and I-55) have exchange rates with standard deviations smaller than a given precision threshold (0.3 on the logarithmic scale), their values are drastically different

from each other (Figure 1C). Our data from adiabatic relaxation dispersion experiments also indicated that these four methyl groups (I-21, I-24, I-36, and I-55) in the effector lobe of GDP-bound KRAS display fast and diverse dynamic behaviors (Figure 1C and Figures S4 and S5). In contrast, our SQ-CPMG data showed that both the calculated exchange rates and the temperature-dependent variations (or Arrhenius slopes) of these four KRAS methyl groups are strikingly similar to one another when in the GMPPNP-bound form (Figure 1C, the curve fitting of relaxation dispersion data is shown in Figure S6). This suggests that a synchronized and collective slow motion of the effector lobe of KRAS dominates its relaxation dispersion profiles when the γ-phosphate is present in the nucleotide pocket. Similarly, three other methyl groups of residues I-100, I-139, and I-142 in the allosteric lobe of KRAS, exhibiting large relaxation dispersion profiles, show slow exchange rates in the GMPPNP-bound form, although their temperature-dependent variations are not similar to one another (Figure 1D, the curve fitting of relaxation dispersion data is shown in Figure S6). In the GDP-bound form (in the absence of γ-phosphate), the detailed analysis of χ^2 surfaces shows no clear temperature-dependent conformational exchange (Figure S4), suggesting that the motions are faster than the detectable timescale of the adiabatic relaxation dispersion experiments. The above results show that the presence of the γ-phosphate in KRAS not only slows down the conformational exchange processes present in the GDP form but also results in a synchronized and collective motion dominant in relaxation dispersion profiles together with other local motions, in contrast to the fast motions sampling more diverse conformational states in the GDP form.

Existence of ms-μ Dynamics in the State I Conformation.

To further understand the complex conformational dynamics of KRAS, we extended our dynamic study to three selected mutants (V29G, T35S, and T35A) known to stabilize the state I conformation in the GMPPNP-bound form of RAS proteins[9,11] (Figure S7). To reveal the existence of possible conformational exchange in the ms-μ timescale, we probed the conformational dynamics of these three mutants in the GMPPNP-bound form using carbon SQ-CPMG experiments (Figure 2A). The resulting data showed that the large relaxation dispersion profiles observed in wild-type KRAS for 7 out of 11 methyl groups are either significantly suppressed or completely quenched by these single mutations, at 25 °C (Figure 2A and Figure S2B). This fact confirms that conformational exchange between state I and state II is the dominant contributor to the relaxation dispersion profiles of wild-type KRAS. Although relaxation dispersion profiles of both T35S and T35A GMPPNP-bound mutants showed no ms-μ motions within the detection limit of the standard CPMG experiments, sizable “residual” relaxation dispersion profiles were observed for some methyl groups (I-21, I-24, I-55, and I-100) in the GMPPNP-bound V29G mutant (Figure 2A). This clearly shows the existence of conformational sub-states within the state I and confirmed the complexity of conformational dynamics of GMPPNP-bound KRAS on the ms-μ timescale.

Interestingly, although the chemical shifts of the selectively labeled methyl groups are highly sensitive to changes in the relative population distribution of state I and state II conformations (Figure S8), only small chemical shift perturbations, exclusively for methyl groups in the proximity of the mutation, and almost no change in the ^{31}P chemical shift of the γ-phosphate were observed among these mutants (Figure 2B and Figure S7).

Since observed chemical shifts represent population averages, our data suggest that there is little difference in the population distributions of the conformational sub-states among these three mutants. The large differences in the amplitudes of temperature-dependent relaxation dispersion profiles observed between V29G and the other two mutants (T35S and T35A) demonstrate that labeled methyl groups in KRAS are sensitive probes to detect conformational dynamics phenomena (Figure 2C) that are otherwise undetectable by chemical shift perturbations. Moreover, we experimentally showed that the previously defined state I conformation of KRAS in the GMPPNP-bound form exhibits multiple sub-states present in both effector and allosteric lobes, with conformational exchange rates in the ms-μs timescale.

Correlation between Effector Binding and Altered Conformational Dynamics.

We wanted to find if slow (ms-μs) conformational dynamics has a role in the effector-binding affinity of KRAS. It is known that the conformational dynamics of proteins contribute to their entropic energy. To understand the thermodynamic contributions to the interaction between GMPPNP-bound KRAS and the RBD of RAF1, our isothermal titration calorimetry (ITC) data showed that the binding event is entropically driven (Figure 3A). (W.T.: K_D = 0.17 ± 0.04 μM; V29G: K_D = 1.09 ± 0.1 μM; T35S: K_D = 7.6 ± 1.3 μM.) The K_D values reported by our ITC experiments (Figure 3A and Figure S9) are consistent with the previously reported binding affinities of wild-type and mutants of HRAS to RAF1-RBD.[9] Interestingly, the binding affinities and entropic contributions of the wild-type, V29G, and T35S mutants to the RBD of RAF1 are qualitatively correlated with the amplitudes of relaxation dispersion profiles by SQ-CPMG experiments (Figure S2B and Figure 2A). Moreover, combining SQ-CPMG data and chemical shift perturbations (Figure 2A,B and Figure S7), we hypothesized that exchange rates among sub-states in the T35S mutant are increased and thus are undetected by standard SQ-CPMG experiments. To validate this, we carried out methyl adiabatic relaxation dispersion experiments to probe faster conformational exchanges in the GMPPNP-bound T35S mutant, and indeed detected these fast exchange rates (Figures S10 and S11). Furthermore, the detailed analysis of reported temperature-dependent conformational exchanges in wild-type, V29G, and T35S mutants of KRAS reveals a striking correlation between ms-μ conformational dynamics and effector-binding affinity of KRAS (Figures 3A,B and Figures S10-S12, the curve fitting of relaxation dispersion data is shown in Figures S6, S11, and S12). In contrast, when compared with ns-ps dynamics of KRAS proteins, no such correlation is observed (Figure S13). Here, if two methyl groups in the same protein exhibit almost identical exchange rates as well as temperature-dependent slopes, we deem them as dynamically coupled. As the entropic contribution decreases with the degree of structural perturbation induced by mutations (Figure 3A), we found that not only the reported exchange rates increase (Figure 3B) but also that the number of observed dynamically coupled methyl groups connecting effector and allosteric lobes decrease (Figure 3C). This trend is further supported by the dynamic data in GDP-bound wild-type KRAS, which exhibits fast and diverse conformational dynamics and shows no binding affinity to the RBD of RAF1 (Figure 1C,D). Together with the entropic-driven binding event of KRAS to the RBD of RAF1, our data show a clear correlation between the binding affinity of KRAS and its altered conformational dynamics.

DISCUSSION AND CONCLUSIONS

Here, we established a set of customized relaxation dispersion experiments[23-25] on selected methyl groups to probe complex ms-μs conformational dynamics in wild-type KRAS with a dominant state II conformation and in KRAS mutants that stabilize the state I conformation. The high sensitivity of these experiments can facilitate systematic studies on various oncogenic mutants, which would be difficult by conventional NMR approaches that use amide groups. While it is expected that the conformational dynamics of KRAS is complex due to the diversity of its interaction partners fulfilling a variety of biological functions, our approach can easily offer insight into the dynamic behaviors without explicitly identifying exchange models of the detected multiple conformational states.[43] Although we detect complex ms-μs conformational dynamics in GMPPNP-bound wild-type KRAS (Figure 1C,D), all the data (Figures 1, 2, and 3) suggest the existence of a synchronized and collected motion connecting both lobes. That motion is induced by the exchange between state I and state II and is dominant in our SQ-CPMG relaxation dispersion profiles (Figure 2A and Figure S2B). More site-specific reporters and detailed studies can be obtained by increasing the number of labeled methyl groups (alanine, leucine, threonine, and valine). While ^{31}P NMR analysis provides valuable information regarding the population distributions between state I and state II conformations, our customized relaxation dispersion techniques provided critical information regarding the energy barriers separating these conformational states. Methyl SQ-CPMG experiments are used to probe millisecond conformational dynamics, while adiabatic relaxation dispersion experiments are employed to detect microsecond conformational dynamics. This combined approach and the associated data analysis used here to efficiently study the conformational dynamics of various KRAS mutants on a broader timescale can be applied to study the complex ms-μs conformational dynamics of other macromolecules. When single mutants stabilizing the state I conformation were systematically investigated by this approach, our relaxation dispersion data detected different ms-μs conformational dynamics among these mutants, which is unapparent when examining chemical shift perturbations (Figure 2). Moreover, our relaxation dispersion data (Figures 1 and 3) show a clear and strong correlation between ms-μs conformational dynamics of KRAS proteins and their binding affinities to RAF1-RBD. Our approach can stimulate further analyses of conformational dynamics variation among RAS oncogenic mutants.

Our ITC measurements on different KRAS mutants showed that there is a wide range of binding affinities to RAF1-RBD even when the state I conformation of KRAS is stabilized. Thus, as shown in Figure 2B and Figure S7, the conformational population distribution (reflected in the NMR spectra) is not sufficient to explain the differences in the binding affinities to RAF1-RBD (Figure 3A). Because this binding event is entropically driven, the altered entropic content of the KRAS mutant can affect the overall entropic contribution of the binding event, assuming that the entropic content of the KRAS complexed with RAF1-RBD is not affected by the mutations. The thermodynamic parameters also showed that almost equal amounts of enthalpic and entropic penalties are introduced by the single mutations, V29G and T35S (Figure 3A). The small changes in enthalpic contribution reflect little structural change by the single mutations, but corresponding changes in entropic

contribution can be easily revealed by large changes in ms-μs conformational dynamics observed using our method (Figure 3). Thus, this approach revealed subtle changes in entropic contribution, which allows a better understanding of a potential fundamental molecular mechanism of KRAS biological functions and can stimulate future studies on the correlation between conformational dynamics and altered biochemical activities in oncogenic mutants.

Supplementary Material

Refer to Web version on PubMed Central for supplementary material.

ACKNOWLEDGMENTS

We thank Julia Cregger, John-Paul Denson, Matt Drew, Min Hong, Jen Mehalko, Shelley Perkins, Nitya Ramakrishnan, Mukul Sherekar, Kelly Snead, and Vanessa Wall for their help in cloning, expressing, and purifying recombinant proteins. We thank Mariam Ashraf for the help with the RAS nucleotide exchange, Jess Li for sharing the high-level deuteration protein expression protocol, and Janusz Koscielniak for his continuous support in maintaining the NMR spectrometers at FNLCR.

Funding

This project was funded in part with federal funds from the National Cancer Institute, the National Institutes of Health, contract no. 75N91019D00024, and the Intramural Research Program. The content of this publication does not necessarily reflect the views or policies of the Department of Health and Human Services, nor does mention of trade names, commercial products, or organizations imply endorsement by the U.S. Government.

REFERENCES

(1). Simanshu DK; Nissley DV; McCormick F RAS Proteins and Their Regulators in Human Disease. Cell 2017, 170, 17–33. [PubMed: 28666118]

(2). Prior IA; Hood FE; Hartley JL The Frequency of Ras Mutations in Cancer. Cancer Res. 2020, 80, 2969–2974. [PubMed: 32209560]

(3). Moore AR; Rosenberg SC; McCormick F; Malek S RAS-targeted therapies: is the undruggable drugged? Nat Rev Drug Discov 2020, 19, 533–552. [PubMed: 32528145]

(4). Ostrem JM; Peters U; Sos ML; Wells JA; Shokat KM K-Ras(G12C) inhibitors allosterically control GTP affinity and effector interactions. Nature 2013, 503, 548–551. [PubMed: 24256730]

(5). Janes MR; Zhang J; Li LS; Hansen R; Peters U; Guo X; Chen Y; Babbar A; Firdaus SJ; Darjania L; Feng J; Chen JH; Li S; Li S; Long YO; Thach C; Liu Y; Zarieh A; Ely T; Kucharski JM; Kessler LV; Wu T; Yu K; Wang Y; Yao Y; Deng X; Zarrinkar PP; Brehmer D; Dhanak D; Lorenzi MV; Hu-Lowe D; Patricelli MP; Ren P; Liu Y Targeting KRAS Mutant Cancers with a Covalent G12C-Specific Inhibitor. Cell 2018, 172, 578–589.e17. [PubMed: 29373830]

(6). Lu S; Jang H; Muratcioglu S; Gursoy A; Keskin O; Nussinov R; Zhang J Ras Conformational Ensembles, Allostery, and Signaling. Chem. Rev 2016, 116, 6607–6665. [PubMed: 26815308]

(7). Pantsar T. The current understanding of KRAS protein structure and dynamics. Comput Struct Biotechnol J 2020, 18, 189–198. [PubMed: 31988705]

(8). Pai EF; Krengel U; Petsko GA; Goody RS; Kabsch W; Wittinghofer A Refined crystal structure of the triphosphate conformation of H-ras p21 at 1.35 A resolution: implications for the mechanism of GTP hydrolysis. EMBO J 1990, 9, 2351–2359. [PubMed: 2196171]

(9). Spoerner M; Herrmann C; Vetter IR; Kalbitzer HR; Wittinghofer A Dynamic properties of the Ras switch I region and its importance for binding to effectors. Proc. Natl. Acad. Sci. U. S. A 2001, 98, 4944–4949. [PubMed: 11320243]

(10). Spoerner M; Nuehs A; Ganser P; Herrmann C; Wittinghofer A; Kalbitzer HR Conformational states of Ras complexed with the GTP analogue GppNHp or GppCH2p: implications for the interaction with effector proteins. Biochemistry 2005, 44, 2225–2236. [PubMed: 15697248]

(11). Spoerner M; Wittinghofer A; Kalbitzer HR Perturbation of the conformational equilibria in Ras by selective mutations as studied by ^{31}P NMR spectroscopy. FEBS Lett. 2004, 578, 305–310. [PubMed: 15589837]

(12). Nassar N; Horn G; Herrmann C; Block C; Janknecht R; Wittinghofer A Ras/Rap effector specificity determined by charge reversal. Nat. Struct. Biol 1996, 3, 723–729. [PubMed: 8756332]

(13). Rosnizeck IC; Spoerner M; Harsch T; Kreitner S; Filchtinski D; Herrmann C; Engel D; Konig B; Kalbitzer HR Metal-bis(2-picolyl)amine complexes as state 1(T) inhibitors of activated Ras protein. Angew Chem Int Ed Engl 2012, 51, 10647–10651. [PubMed: 22996816]

(14). Rosnizeck IC; Filchtinski D; Lopes RP; Kieninger B; Herrmann C; Kalbitzer HR; Spoerner M Elucidating the mode of action of a typical Ras state 1(T) inhibitor. Biochemistry 2014, 53, 3867–3878. [PubMed: 24866928]

(15). O'Connor C; Kovrigin EL Global conformational dynamics in ras. Biochemistry 2008, 47, 10244–10246. [PubMed: 18771285]

(16). Long D; Marshall CB; Bouvignies G; Mazhab-Jafari MT; Smith MJ; Ikura M; Kay LE A comparative CEST NMR study of slow conformational dynamics of small GTPases complexed with GTP and GTP analogues. Angew Chem Int Ed Engl 2013, 52, 10771–10774. [PubMed: 24039022]

(17). Mao Y; Yao H; Wang H; Cheng P; Long D Microsecond Timescale Dynamics of GDP-Bound Ras Underlies the Formation of Novel Inhibitor-Binding Pockets. Angew Chem Int Ed Engl 2016, 55, 15629–15632. [PubMed: 27860047]

(18). Toyama Y; Kontani K; Katada T; Shimada I Conformational landscape alternations promote oncogenic activities of Ras-related C3 botulinum toxin substrate 1 as revealed by NMR. Sci. Adv 2019, 5, No. eaav8945. [PubMed: 30891502]

(19). Johnson CW; Reid D; Parker JA; Salter S; Knihtila R; Kuzmic P; Mattos C The small GTPases K-Ras, N-Ras, and H-Ras have distinct biochemical properties determined by allosteric effects. J Biol Chem 2017, 292, 12981–12993. [PubMed: 28630043]

(20). Kalbitzer HR; Spoerner M; Ganser P; Hozsa C; Kremer W Fundamental link between folding states and functional states of proteins. J. Am. Chem. Soc 2009, 131, 16714–16719. [PubMed: 19856908]

(21). Kalbitzer HR; Rosnizeck IC; Munte CE; Narayanan SP; Kropf V; Spoerner M Intrinsic allosteric inhibition of signaling proteins by targeting rare interaction states detected by high-pressure NMR spectroscopy. Angew Chem Int Ed Engl 2013, 52, 14242–14246. [PubMed: 24218090]

(22). Wang X. Conformational Fluctuations in GTP-Bound K-Ras: A Metadynamics Perspective with Harmonic Linear Discriminant Analysis. J. Chem. Inf. Model 2021, 61, 5212–5222. [PubMed: 34570515]

(23). Lundstrom P; Vallurupalli P; Religa TL; Dahlquist FW; Kay LE A single-quantum methyl C-13-relaxation dispersion experiment with improved sensitivity. J. Biomol NMR 2007, 38, 79–88. [PubMed: 17464570]

(24). Chao FA; Li Y; Zhang Y; Byrd RA Probing the Broad Time Scale and Heterogeneous Conformational Dynamics in the Catalytic Core of the Arf-GAP ASAP1 via Methyl Adiabatic Relaxation Dispersion. J. Am. Chem. Soc 2019, 141, 11881–11891. [PubMed: 31293161]

(25). Chao FA; Khago D; Byrd RA Achieving pure spin effects by artifact suppression in methyl adiabatic relaxation experiments. J. Biomol. NMR 2020, 74, 223–228. [PubMed: 32333192]

(26). Tugarinov V; Kay LE Ile, Leu, and Val methyl assignments of the 723-residue malate synthase G using a new labeling strategy and novel NMR methods. J. Am. Chem. Soc 2003, 125, 13868–13878. [PubMed: 14599227]

(27). Dharmaiah S; Tran TH; Messing S; Agamasu C; Gillette WK; Yan W; Waybright T; Alexander P; Esposito D; Nissley DV; McCormick F; Stephen AG; Simanshu DK Structures of N-terminally processed KRAS provide insight into the role of N-acetylation. Sci. Rep 2019, 9, 10512. [PubMed: 31324887]

(28). Taylor T; Denson JP; Esposito D Optimizing Expression and Solubility of Proteins in E. coli Using Modified Media and Induction Parameters. Methods Mol. Biol 2017, 1586, 65–82. [PubMed: 28470599]

(29). Kopra K; Vuorinen E; Abreu-Blanco M; Wang Q; Eskonen V; Gillette W; Pulliainen AT; Holderfield M; Harma H Homogeneous Dual-Parametric-Coupled Assay for Simultaneous Nucleotide Exchange and KRAS/RAF-RBD Interaction Monitoring. Anal Chem. 2020, 92, 4971–4979. [PubMed: 32106676]

(30). Delaglio F; Grzesiek S; Vuister GW; Zhu G; Pfeifer J; Bax A NMRPipe: a multidimensional spectral processing system based on UNIX pipes. J. Biomol NMR 1995, 6, 277–293. [PubMed: 8520220]

(31). Lee W; Tonelli M; Markley JL NMRFAM-SPARKY: enhanced software for biomolecular NMR spectroscopy. Bioinformatics 2015, 31, 1325–1327. [PubMed: 25505092]

(32). Sun H; Kay LE; Tugarinov V An optimized relaxation-based coherence transfer NMR experiment for the measurement of side-chain order in methyl-protonated, highly deuterated proteins. J Phys Chem B 2011, 115, 14878–14884. [PubMed: 22040035]

(33). Lee D; Hilty C; Wider G; Wuthrich K Effective rotational correlation times of proteins from NMR relaxation interference. J. Magn. Reson 2006, 178, 72–76. [PubMed: 16188473]

(34). Baldwin AJ An exact solution for R2,eff in CPMG experiments in the case of two site chemical exchange. J. Magn. Reson 2014, 244, 114–124. [PubMed: 24852115]

(35). Bieri M; Gooley PR Automated NMR relaxation dispersion data analysis using NESSY. Bmc Bioinformatics 2011, 12, 421. [PubMed: 22032230]

(36). Maciejewski MW; Schuyler AD; Gryk MR; Moraru II; Romero PR; Ulrich EL; Eghbalnia HR; Livny M; Delaglio F; Hoch JC, NMRbox: A Resource for Biomolecular NMR Computation. Biophys. J 2017, 112, 1529–1534. [PubMed: 28445744]

(37). Karunanithy G; Shukla VK; Hansen DF Methodological advancements for characterising protein side chains by NMR spectroscopy. Curr. Opin. Struct. Biol 2021, 70, 61–69. [PubMed: 33989947]

(38). Sheppard D; Sprangers K; Tugarinov V Experimental approaches for NMR studies of side-chain dynamics in high-molecular-weight proteins. Prog. Nucl. Magn. Reson. Spectrosc 2010, 56, 1–45. [PubMed: 20633347]

(39). Fang Z; Lee KY; Huo KG; Gasmi-Seabrook G; Zheng L; Moghal N; Tsao MS; Ikura M; Marshall CB Multivalent assembly of KRAS with the RAS-binding and cysteine-rich domains of CRAF on the membrane. Proc. Natl. Acad. Sci. U. S. A 2020, 117, 12101–12108. [PubMed: 32414921]

(40). Mazhab-Jafari MT; Marshall CB; Smith MJ; Gasmi-Seabrook GMC; Stathopulos PB; Inagaki F; Kay LE; Neel BG; Ikura M Oncogenic and RASopathy-associated K-RAS mutations relieve membrane-dependent occlusion of the effector-binding site. Proc. Natl. Acad. Sci. U. S. A 2015, 112, 6625–6630. [PubMed: 25941399]

(41). Korzhnev DM; Kloiber K; Kanelis V; Tugarinov V; Kay LE Probing slow dynamics in high molecular weight proteins by methyl-TROSY NMR spectroscopy: application to a 723-residue enzyme. J. Am. Chem. Soc 2004, 126, 3964–3973. [PubMed: 15038751]

(42). Chao F-A; Byrd RA Protein dynamics revealed by NMR relaxation methods. Emerging Topics in Life Sciences 2018, 2, 93–105.

(43). Chao FA; Zhang Y; Byrd RA Theoretical classification of exchange geometries from the perspective of NMR relaxation dispersion. J. Magn. Reson 2021, 328, 107003. [PubMed: 34058714]

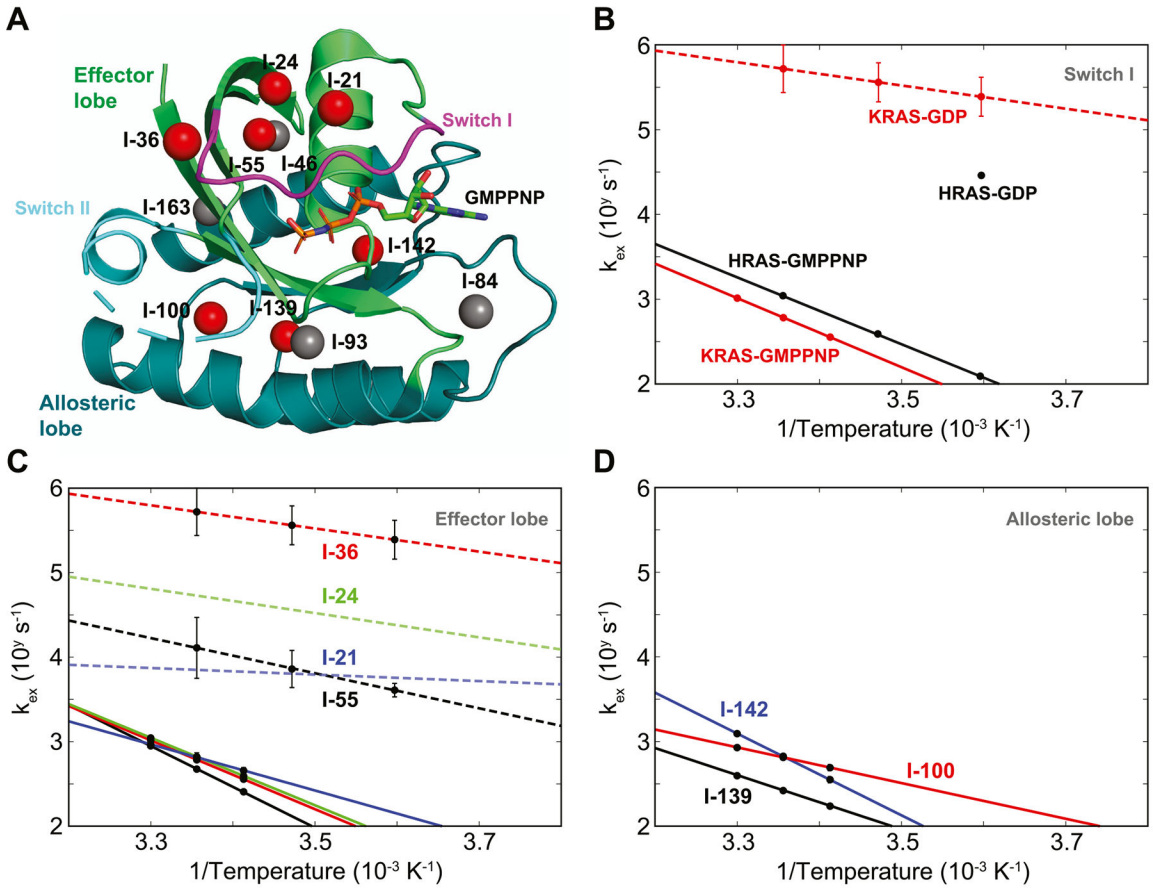

Figure 1.

Temperature-dependent conformational dynamics of wild-type KRAS on a ms-μtimescale studied by δ_1-labeled methyl groups of isoleucine residues. The solid-line and dash-line data for wild-type KRAS were generated from SQ-CPMG experiments and adiabatic relaxation dispersion experiments, respectively. (A) Isotope-labeled methyl groups with large relaxation dispersion profiles at 25 °C in GMPPNP-bound KRAS are marked as red spheres in the crystal structure (PDB: 6VC8), while others are marked as gray spheres. The effector lobe (residues 1–86) and the allosteric lobe (residues 87–166) are shown in light green and dark green, respectively. The switch I (residues 30–38) and switch II (residues 60–76) are shown in magenta and cyan, respectively. (B) Temperature-dependent exchange rates of the methyl group at I-36 in both GDP-bound and GMPPNP-bound KRAS are plotted as red data points, while the published results on HRAS are plotted as black data points. (C) Temperature-dependent exchange rates of four methyl groups (from I-21, I-24, I-36, and I-55) in the effector lobe in GDP-bound and GMPPNP-bound KRAS are plotted as dashed lines and solid lines, respectively. Residues I-21, I-24, I-36, and I-55 are shown in blue, green, red, and black, respectively. The data points for I-21 and I-24 in the GDP-bound form are not shown due to their large standard deviations, and only interpolating dashed lines are shown as trends in this panel. (D) Temperature-dependent exchange rates of three methyl groups in the allosteric lobe (residues I- 100, I-139, and I-142 in red, black, and blue, respectively) are only available in the GMPPNP-bound KRAS and are plotted as solid lines.

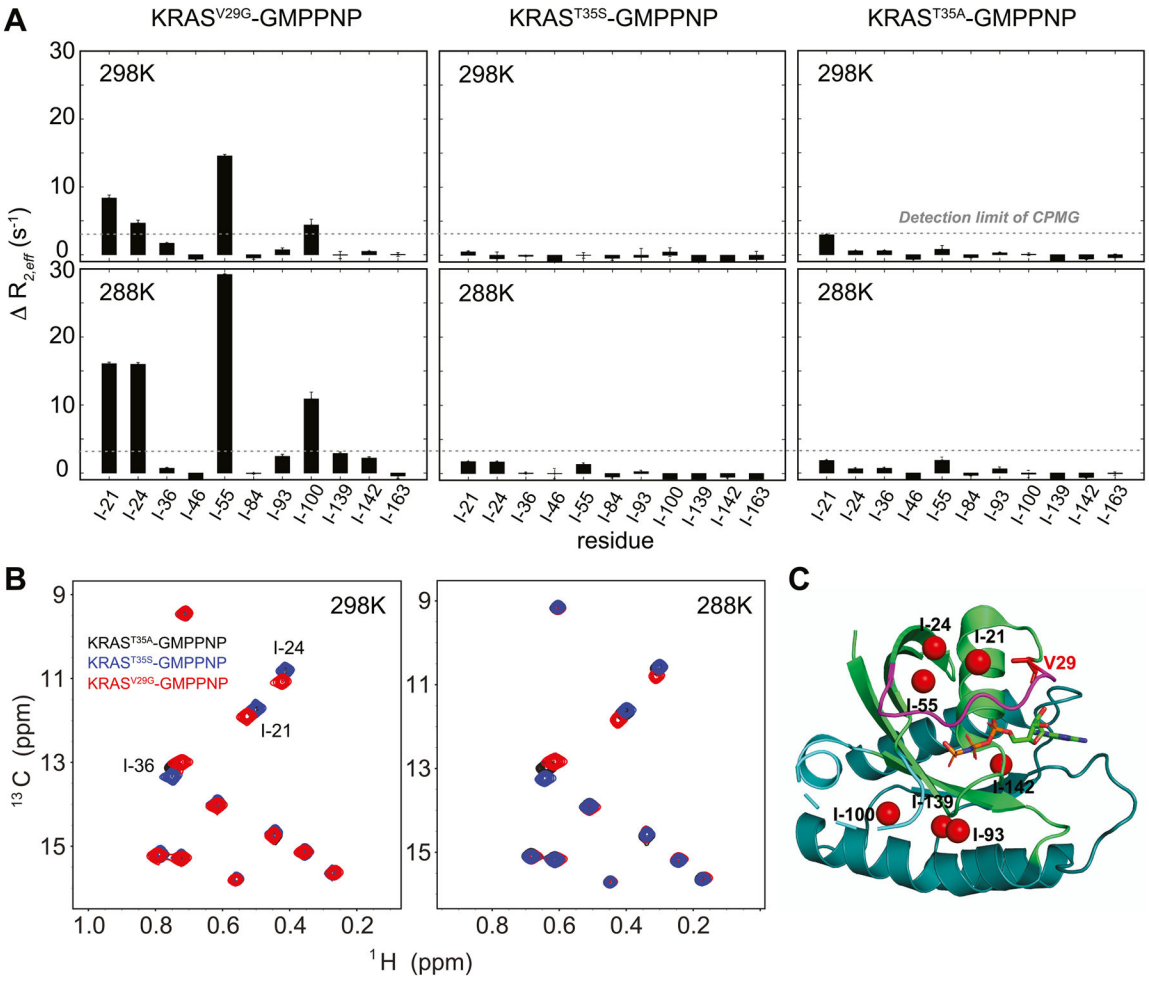

Figure 2.

Conformational dynamics in the state I conformation revealed by relaxation dispersion experiments. (A) Amplitudes of relaxation dispersion profiles from carbon SQ-CPMG with a 20 ms constant time at different temperatures are plotted for different KRAS mutants. The amplitudes are calculated using differences between R_{2eff} values at νCPMG frequencies of 100 and 1000 Hz. (B) Methyl-TROSY spectra of different KRAS mutants at different temperatures are overlaid, and only perturbed methyl resonances are labeled. $KRAS^{V29G}$, $KRAS^{T35s}$, and $KRAS^{T35a}$ are shown in red, blue, and black, respectively. (C) Methyl groups showing temperature-dependent conformational dynamics in the $KRAS^{V29G}$ mutant are marked as red spheres in the crystal structure of KRAS (PDB: 6VC8).

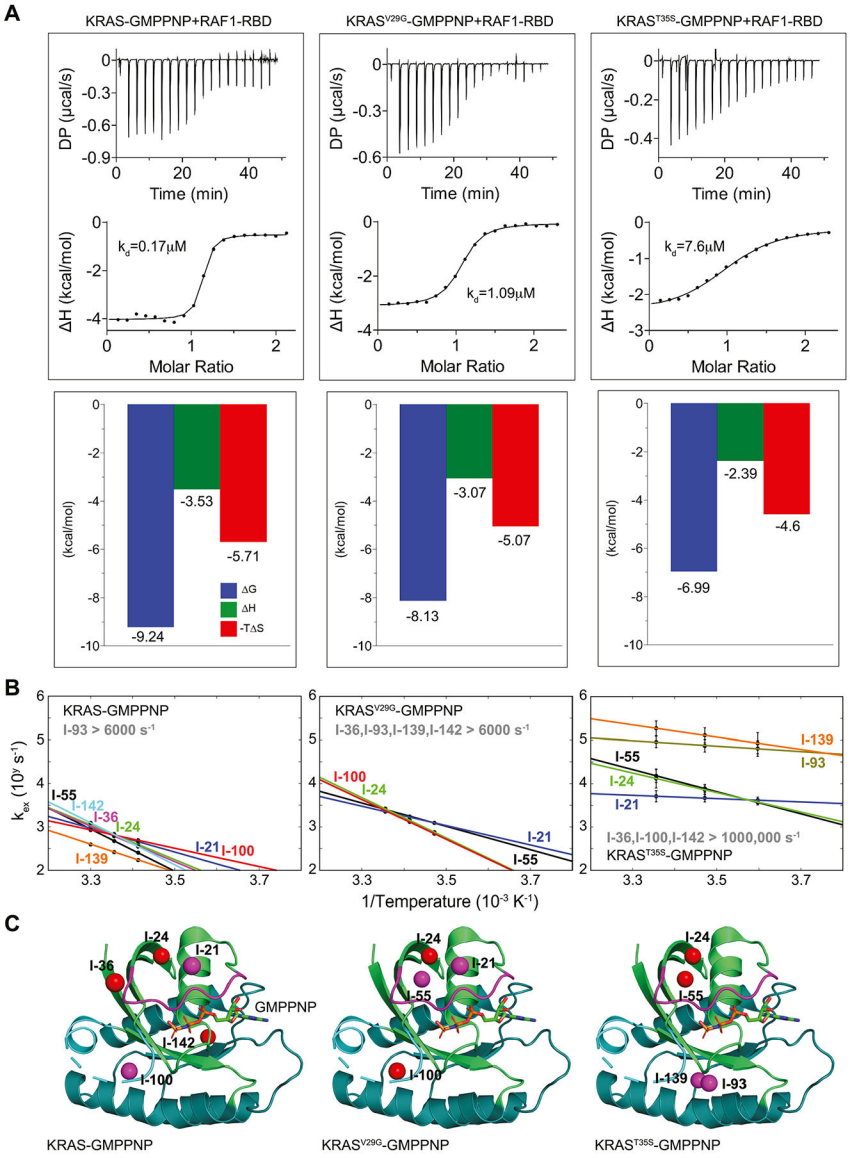

Figure 3.

Correlation between ms-μ conformational dynamics and binding affinity of KRAS mutants with the RAF1 effector. (A) Binding affinities and thermodynamic parameters obtained by ITC measurements between GMPPNP-bound KRAS and RAF1-RBD. (B) Measurable temperature-dependent exchange rates of methyl groups are plotted for KRAS, KRAS^{V29G}, and KRAS^{T35S} mutants. Data for both KRAS and KRAS^{V29G} mutant were generated by SQ-CPMG, and KRAS^{T35s} mutant data were generated by adiabatic relaxation dispersion experiments. Residues I-21, I-24, I-36, I-55, I-93, I-100, I-139, and I-142 are shown in blue, green, purple, black, dark green, red, orange, and cyan, respectively. (C) Methyl groups with similar exchange rates and temperature-dependent variations (or Arrhenius slopes) are shown as spheres with the same color (red or purple) in the crystal structure of KRAS (PDB: 6VC8).